Gold-layered calcium phosphate plasmonic resonants for localized photothermal treatment of human epithelial cancer†

Jinyoung Kang,[ab] Jaemoon Yang,[ac] Jaewon Lee,[a] Seung Jae Oh,[c] Seyoung Moon,[bf] Hong Jae Lee,[d] Sang Cheon Lee,[d] Joo-Hiuk Son,[e] Donghyun Kim,[f] Kwangyeol Lee,[g] Jin-Suck Suh,[c] Yong-Min Huh*[c] and Seungjoo Haam*[a]

Received 19th December 2008, Accepted 24th March 2009
First published as an Advance Article on the web 6th April 2009
DOI: 10.1039/b822835c

We fabricated *de novo* biocompatible mineral plasmon resonants for localized and systemic treatment of cancer. Biodegradable calcium-phosphate gold nanocomposites were synthesized for inducing a superior surface plasmon resonance effect. The combination of therapeutic antibody, Erbitux® and NIR laser with nanocomposites demonstrated the potential for selective bimodal cancer treatment by combination of EGFR-induced signaling inhibition as a systemic treatment and localized photothermal effects caused by the NIR laser.

Surface plasmon resonance (SPR) effects from noble metal nanostructures have emerged as a highly promising localized photothermal cancer therapy.[1–4] In particular, the plasmonic gold nanostructures such as core-shell nanocomposites,[5–8] nanorods[9–11] and nanocages[12–15] have recently been developed because they can strongly absorb near infrared (NIR) light for localized heating to ablate the cancer cells without damage to normal tissue or blood.[16] For highly selective and efficient photothermal cancer therapy, thus, the synthesis of well-tailored gold nanostructures is vital for: (i) enhanced plasmon resonance effect by NIR light for sufficient photothermal effect with minimal dose amounts,[17] (ii) biocompatibility for a reduction in unwanted immune responses,[18] (iii) targeted delivery to the specific cancerous cells by bio-conjugation with a targeting moiety to mitigate the damage to healthy tissue[19] and (iv) collapse of resonant structure after photothermal treatment to reduce the side effects from unnecessary NIR light.[20] Furthermore, the use of a therapeutic antibody, which inhibits the metabolism of cancer cells for growth and proliferation, may increase the systemic treatment efficacy when combined with localized photothermal effect from gold nanostructures.[21]

Herein, we report a novel strategy for bimodal cancer treatment using a biocompatible mineral plasmon resonant for a localized photothermal treatment and a therapeutic antibody for a systemic treatment (Fig. 1). To prepare calcium phosphate-gold nanocomposites (CPGNs) as photothermal agents, mineral calcium phosphate nanoparticles (CPNs) were synthesized as dielectric cores because CPNs are highly biocompatible and biodegradable in the lysosomal site of a cell due to a low pH (<4) in comparison to conventional silica nanoparticles.[21–23] After all, conventional silica nanoparticles are not degradable under a proton-rich intracellular environment, while CPNs can be easily dissolved by protons with calcium and phosphate ions. Besides, cancer cells provide more acidic environments compared to normal cells. Subsequently, the surface of CPNs is modified to provide amine groups for a generation of a gold nano-layer by the seed-mediated growth method (Fig. 1a).[24] Furthermore, CPGNs are linked with a chimeric humanized monoclonal antibody, Erbitux® (ERB), for targeting toward the epidermal growth factor receptor (EGFR) and an additional therapeutic effect by inhibition of the EGFR signaling pathway, a key pathway for a carcinogenesis (Fig. 1b).[25,26]

CPNs were synthesized by a chemical precipitation method[27,28] and their ellipsoidal morphology was confirmed by a transmission electron microscope (TEM) image (see ESI†). For generation of a gold overlayer on the surface of the CPNs, we modified the hydroxyl

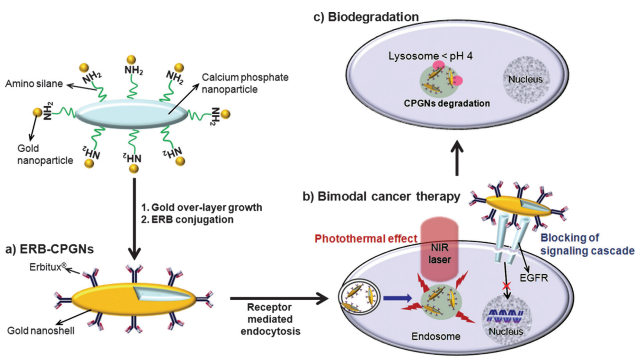

Fig. 1 Conceptual illustration for localized and systemic cancer treatment using intelligent mineral plasmon resonants; a) anti-EGFR antibody (Erbitux®, ERB) conjugation onto calcium phosphate-gold nanocomposites (CPGNs), b) bimodal cancer treatment using ERB-CPGNs and NIR laser, and c) biodegradation of CPGNs after treatments.

[a]*Department of Chemical and Biomolecular Engineering, Yonsei University, Seoul, 120-749, Republic of Korea. Fax: +82-2-312-6401; Tel: +82-2-2123-2751*
[b]*Program for Nanomedical Science and Technology, Yonsei University, Seoul, 120-749, Republic of Korea*
[c]*Department of Radiology, College of Medicine, Yonsei University, Seoul, 120-752, Republic of Korea*
[d]*Department of Oral Biology & Institute of Oral Biology, School of Dentistry, Kyung Hee University, Seoul, 130-701, Republic of Korea*
[e]*Department of Physics, University of Seoul, Seoul, 130-743, Republic of Korea*
[f]*Department of Electrical and Electronic Engineering, Yonsei University, Seoul, 120-749, Republic of Korea*
[g]*Department of Chemistry, Korea University, Seoul, 136-701, Republic of Korea*
† Electronic supplementary information (ESI) available: Further experimental details. See DOI: 10.1039/b822835c

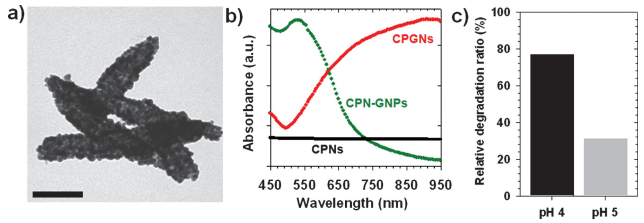

Fig. 2 a) TEM image of CPGNs (scale bar means 100 nm). b) UV-Vis absorbance spectra of CPNs, CPNs-GNPs and CPGNs. The characteristic absorbance of CPGNs was shifted to the NIR region due to the formation of the gold overlayer. c) Relative degradation ratio of CPGNs at pH 4 and 5 compared to the concentration of calcium ion at pH 7.4.

groups on the surface of CPNs with amine groups using 3-aminopropyl trimethoxysilane (APTMS) and the amine groups of aminated CPNs were verified at 400.7 eV (N 1s) by X-ray photoelectron spectroscopy (ESI†). To generate nucleation sites for the formation of the gold overlayer, gold nanoparticles (GNPs, ~2 nm) were synthesized as seeds by the gold salt reduction method and were attached on the surface of CPNs by electrostatic interaction between the amine group and gold (CPNs-GNPs, ESI†). Then, ellipsoidal CPGNs were successfully synthesized after the growth of the reticular gold overlayer on the surface of CPNs by the gradual reduction of gold salts. In Fig. 2a, the TEM image indicates the ellipsoidal morphology with an aspect ratio of *ca.* 4.7, which was smaller than that of naked CPNs (*ca.* 6.5) due to generation of the 10 nm thick nanolayer on CPNs. We then performed an elemental analysis of CPNs-GNPs and CPGNs for Ca, P and Au atoms by energy-dispersive X-ray spectroscopy and found that Au components were increased from ~5.0% (CPNs-GNPs) to ~37.2% (CPGNs) after the complete formation of the gold nanolayer on the surface of the CPNs-GNPs (ESI†). From the X-ray diffraction pattern of the CPGNs, moreover, we observed that the characteristic features of the CPNs had vanished after the CPNs were fully covered by the gold nanolayer (ESI†). To further investigate the optical plasmon peak of the CPGNs, we used a UV-Vis spectrometer to obtain the absorption spectra. The maximum absorbance of CPNs-GNPs was observed at 530 nm and was red-shifted to 920 nm after the gold nanolayer formation (CPGNs) due to the SPR effect (Fig. 2b). Since the geometrical characteristics of the CPGNs included an ellipsoidal shape and core/overlayer structure, we expected a higher SPR effect through the combination of two plasmonic properties arising from i) the oscillation of electrons along the longitudinal and transverse axes of ellipsoidal CPGNs and ii) hybridized plasmons on the inner surface of the layer and the outer layer surface (core/overlayer).[29] From a comparative study of the calculated extinction spectra for ellipsoidal and spherical CPGN, and spherical gold-silica core-layer (ESI†), we observed the plasmon peak of the ellipsoidal CPGN in the NIR region (700–1000 nm). Moreover, a simulation study demonstrated that ellipsoidal CPGNs produce a sufficiently strong SPR effect in the NIR region rather than spherical CPGNs and conventional silica-gold nanoshell structures (ESI†).

To evaluate the biodegradability of CPGNs, UV-Vis absorption spectra of CPGNs under various pH conditions were analyzed for 5 days (ESI†). During the fabrication of the gold overlayer, the attached gold nanoparticles as seeds on the surface of CPNs were grown by a reduction process using tetrachlorolaurate(III) trihydrate and formaldehyde. This consequently led to the formation of a continuous and reticular gold overlayer (ESI†).[8] Thus, CPNs can be degraded under an acidic environment like the intracellular lysosomal site. After exposure to the excess protons, the main peak of CPGNs in the NIR region was blue-shifted under the acidic environment and the absorbance was also decreased due to degradation of CPNs (Fig. 1c and ESI†). Moreover, the relative degradation ratio of CPGNs at pH 4 compared to pH 7.4 was 77.3% calculated using the relative concentration of released calcium ions, which is obtained by inductively coupled plasma mass spectrometry (Fig. 2c). Therefore, CPGNs internalized into cancer cells can be degraded in an acidic biological environment and reduce possible side effects such as unwanted immune responses and unnecessary photothermal effects.

For targeted delivery of CPGNs toward cancer cells, the anti-EGFR antibody, ERB, was conjugated on to the surface of the CPGNs by an electrostatic interaction between CPGNs and the N terminus of the antibody.[30] The colloidal stability of prepared ERB-CPGNs was determined from their resistance to sodium chloride and pH-induced aggregation using laser scattering (ESI†). ERB-CPGNs continuously maintained stable conditions even after 2 weeks because negatively charged ERB-CPGNs (around −20 mV) were stabilized in the aqueous phase by electrostatic repulsion. Twenty equivalent ERBs were conjugated on the surface of CPGN as evaluated using a bicinchoninic acid (BCA) protein assay kit (Pierce). Subsequently, the targeting efficiencies of ERB-CPGNs for EGFR-abundant A431 cells and EGFR-deficient MCF7 cells were evaluated by fluorescence activated cell sorting analysis. Herein, CPGNs were conjugated with human IgG as an irrelevant antibody (IRR-CPGNs) for the control experiment. In Fig. 3a, ERB-CPGNs for A431 cells exhibited 171 times higher targeting potential than IRR-CPGNs due to the binding affinity of anti-EGFR antibody, ERB for EGFR (*$p < 0.01$) and A431 cells treated with ERB-CPGNs demonstrated 216 times stronger fluorescence intensity than MCF7 cells treated with ERB-CPGNs due to the difference in EGFR expression level between A431 and MCF7 cells (**$p < 0.01$). In addition, the confocal microscopic image indicated a remarkable cellular affinity of ERB-CPGNs and receptor-mediated endocytosis into A431 cells (ESI†). The fluorescent green color from ERB-CPGNs was clearly observed around nuclei stained with 4′,6-diamidino-2-phenylindole. The successful internalization of ERB-CPGNs into A431 cells could be also observed by TEM imaging (Fig. 3b). Therefore, ERB-CPGNs

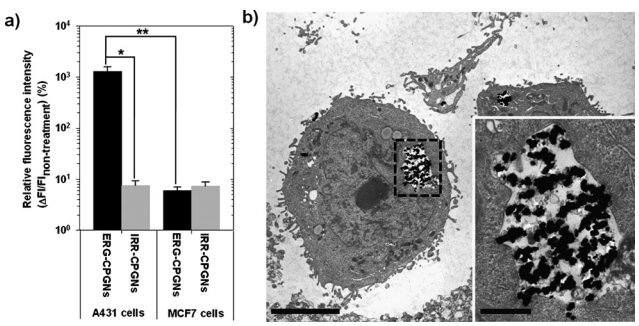

Fig. 3 a) Relative fluorescence intensity ($\Delta FI/FI_{non\text{-}treatment}$, FI: fluorescence intensity) by FACS analysis for A431 and MCF7 cells treated with ERB-CPGNs and IRR-CPGNs, respectively (* and **: $p < 0.01$). b) TEM image of A431 cells treated with ERB-CPGNs (scale bar means 5 μm). ERB-CPGNs were internalized by receptor-mediated endocytosis, and appear as black dots. The inset is a high magnification image (scale bar means 1 μm).

provided abundant possibilities for effective localized photothermal and systemic treatment of cancer.

In order to assess the therapeutic efficacies of ERB-CPGNs as cancer cell ablation agents, A431 or MCF7 cells were incubated with ERB-CPGNs and IRR-CPGNs (100 μg) for 4 hours in the well plates (4×10^3 cells/well). Each incubated cell was then washed for elimination of un-reacted CPGNs and further incubated for 72 hours. After NIR laser exposure (820 nm and 25 W/cm^2 for 5 minutes), the cell viabilities were evaluated using the calcein AM (1 μM) staining method.[31] Calcein AM is a membrane-permeant green fluorescent cell marker that is hydrolyzed by endogenous esterase, and consequently emits fluorescence in the cytoplasm of live cells. In Fig. 4a, ERB-CPGNs partially inhibited the EGFR signaling pathways for growth and proliferation of A431 cells in comparison to only A431 cells irradiated by a NIR laser. After irradiation using a NIR laser (820 nm and 25 W/cm^2 for 5 minutes) of A431 cells treated with ERB-CPGNs, generated photothermal heat from CPGNs increased the temperature up to 49.7 °C within 5 minutes. This effective photothermal phenomenon comes from the strong SPR effect of ellipsoidal CPGNs that was sufficient to denature the intracellular proteins, thus converting the exposure site to a dark color for A431 cells treated with ERB-CPGNs. The results demonstrated that the photothermal phenomena using CPGNs can be easily generated with a small dose of CPGNs and low power source compared to silica based gold nanoshells.[21] For quantification of the therapeutic efficacies for the combination of ERB-CPGNs and NIR laser, furthermore, cell viabilities of A431 and MCF7 cells treated with ERB-CPGNs or IRR-CPGNs under NIR laser irradiation or in the absence of NIR laser exposure were further investigated by MTT assay (Fig. 4b). The therapeutic efficacy of ERB-CPGNs without laser irradiation on A431 cells was approximately 57.0 ± 0.8%, 4.2 times higher compared to the experiment of NIR laser irradiation only. Moreover, the therapeutic efficacy by ERB-CPGNs under NIR laser irradiation (820 nm and 25 W/cm^2 for 5 minutes) for A431 cells was 77.0% (*$p < 0.01$). In contrast, EGFR-deficient MCF7 cell lines treated with ERB-CPGNs or IRR-CPGNs exhibited insignificant therapeutic efficacies, even after NIR laser exposure. These results demonstrate that the combination of ERB-CPGNs and NIR laser can achieve the bimodal treatment of cancer by localized photothermal therapy from the SPR effect of CPGNs and systemic treatment from the inhibition of cellular signaling transduction of cancer cells.

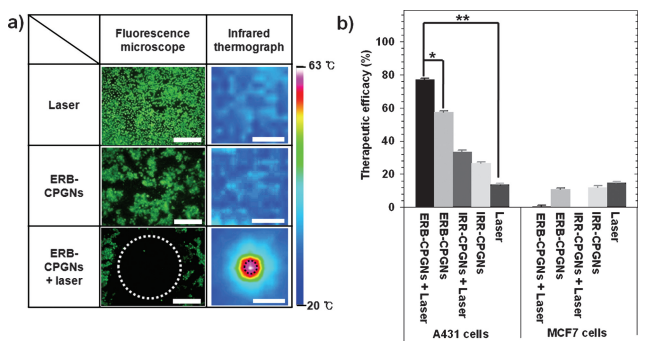

Fig. 4 a) Fluorescence microscopic images of A431 cells stained with calcein AM after treatment with laser only, ERB-CPGNs and ERB-CPGNs + laser (scale bar means 1 mm) (first column). Infrared thermographic images of A431 cells treated with laser only, ERB-CPGNs and ERB-CPGNs + laser (scale bar means 500 μm) (second column). In the last row, the dotted circle indicates the NIR laser exposure area. b) Therapeutic efficacy assessed by MTT assay in A431 or MCF7 cells incubated with ERB-CPGNs and IRR-CPGNs, with or without exposure to the NIR laser (* and **: $p < 0.01$).

Conclusions

In summary, we have successfully formulated ERB-CPGNs as bimodal therapeutic agents for effective epithelial cancer therapy. CPGNs have ellipsoidal CPNs as the dielectric core and an outer gold nanolayer, which makes them high-efficient SPR-inducing plasmonic materials for hyperthermia. The biodegradation capability of CPNs is well suited for applications in the biomedical field. The anti-EGFR antibody, ERB, when conjugated on the surface of ERB-CPGNs efficiently inhibited the growth and proliferation of EGFR-abundant cancer cells and displayed remarkable selectivity. In the future, *in vivo* study will be essential to verify extra uncertain parameters such as thermal ablation efficacy of solid tumors, NIR light penetration depth, biodegradability and blood circulation as well as bio-distribution. We envision that biocompatible plasmonic CPGNs could improve nano-medicinal potential for better treatment of cancer among possible photothermal therapeutic methodologies.

Acknowledgements

This study was supported by a grant of the Korea Healthcare technology R&D Project, Ministry of Health, Welfare & Family Affairs, Republic of Korea (A080661).

Notes and references

1 M. C. Daniel and D. Astruc, *Chem. Rev.*, 2004, **104**, 293–346.
2 M. A. El-Sayed, *Accounts Chem. Res.*, 2001, **34**, 257–264.
3 W. J. Parak, D. Gerion, T. Pellegrino, D. Zanchet, C. Micheel, S. C. Williams, R. Boudreau, M. A. L. Gros, C. A. Larabell and A. P. Alivisatos, *Nanotechnology*, 2003, **14**, R15–R27.
4 Y. Xia, N. J. Halas and G. Editors, *MRS Bull.*, 2005, **30**, 338–348.
5 C. Graf and A. van Blaaderen, *Langmuir*, 2002, **18**, 524–534.
6 L. R. Hirsch, R. J. Stafford, J. A. Bankson, S. R. Sershen, B. Rivera, R. E. Price, J. D. Hazle, N. J. Halas and J. L. West, *Proc. Natl. Acad. Sci. USA*, 2003, **100**, 13549–13554.
7 C. Loo, A. Lowery, N. Halas, J. West and R. Drezek, *Nano Lett.*, 2005, **5**, 709–711.
8 V. Salgueirino-Maceira, M. A. Correa-Duarte, M. Farle, A. Lopez-Quintela, K. Sieradzki and R. Diaz, *Chem. Mat.*, 2006, **18**, 2701–2706.
9 N. R. Jana, L. Gearheart and C. J. Murphy, *J. Phys. Chem. B*, 2001, **105**, 4065–4067.
10 S. Link and M. A. El-Sayed, *J. Phys. Chem. B*, 1999, **103**, 8410–8426.
11 J. Pérez-Juste, I. Pastoriza-Santos, L. M. Liz-Marz and P. Mulvaney, *Coord. Chem. Rev.*, 2005, **249**, 1870–1901.
12 J. Chen, F. Saeki, B. J. Wiley, H. Cang, M. J. Cobb, Z. Y. Li, L. Au, H. Zhang, M. B. Kimmey, X. Li and Y. Xia, *Nano Lett.*, 2005, **5**, 473–477.
13 J. Chen, D. Wang, J. Xi, L. Au, A. Siekkinen, A. Warsen, Z. Y. Li, H. Zhang, Y. Xia and X. Li, *Nano Lett.*, 2007, **7**, 1318–1322.
14 J. Chen, F. Saeki, B. J. Wiley, H. Cang, M. J. Cobb, Z. Y. Li, L. Au, H. Zhang, M. B. Kimmey, X. D. Li and Y. Xia, *Nano Lett.*, 2005, **5**, 473–477.
15 J. Chen, D. Wang, J. Xi, L. Au, A. Siekkinen, A. Warsen, Z. Y. Li, H. Zhang, Y. Xia and X. Li, *Nano Lett.*, 2007, **7**, 1318–1322.
16 J. M. Stern, J. Stanfield, Y. Lotan, S. Park, J. T. Hsieh and J. A. Cadeddu, *J. Endourol.*, 2007, **21**, 939–943.
17 W. W. Minuth, M. Sittinger and S. Kloth, *Cell Tissue Res.*, 1997, **291**, 1–11.
18 C. L. Kenneth, *Adv. Mater.*, 1991, **3**, 87–93.
19 A. R. Lowery, A. M. Gobin, N. J. Halas and J. L. West, *AACR Meeting Abstracts*, 2006, **2006**, B83.

20 T. S. Troutman, J. K. Barton and M. Romanowski, *Adv. Mater.*, 2008, **20**, 2604–2608.
21 J. Lee, J. Yang, H. Ko, S. Oh, J. Kang, J. Son, K. Lee, S. W. Lee, H. G. Yoon, J. S. Suh, Y. M. Huh and S. Haam, *Adv. Funct. Mater.*, 2008, **18**, 258–264.
22 X. Wang, A. Klocke, B. Mihailova, L. Tosheva and U. Bismayer, *J. Phys. Chem. B*, 2008, **112**, 8840–8848.
23 Q. Xu, Y. Tanaka and J. T. Czernuszka, *Biomaterials*, 2007, **28**, 2687–2694.
24 T. Pham, J. B. Jackson, N. J. Halas and T. R. Lee, *Langmuir*, 2002, **18**, 4915–4920.
25 J. Downward, *Nat. Rev. Cancer*, 2003, **3**, 11–22.
26 A. Huether, M. Höpfner, V. Baradari, D. Schuppan and H. Scherübl, *Biochem. Pharmacol.*, 2005, **70**, 1568–1578.
27 H. J. Lee, H. W. Choi, K. J. Kim and S. C. Lee, *Chem. Mat.*, 2006, **18**, 5111–5118.
28 M. Vallet-Regi and D. Arcos, *J. Mater. Chem.*, 2005, **15**, 1509–1516.
29 H. Wang, D. W. Brandl, F. Le, P. Nordlander and N. J. Halas, *Nano Lett.*, 2006, **6**, 827–832.
30 D. Pissuwan, C. Cortie, S. Valenzuela and M. Cortie, *Gold Bull.*, 2007, **40**, 121–129.
31 A. Eneroth, E. Åström, J. Hoogstraate, D. Schrenk, S. Conrad, H. M. Kauffmann and K. Gjellan, *Eur. J. Pharm. Sci.*, 2001, **12**, 205–214.

Supplementary material (ESI) for Journal of Materials Chemistry

Gold-layered Calcium Phosphate Plasmonic Resonants for Localized Photothermal Treatment of Human Epithelial Cancer

Jinyoung Kang, Jaemoon Yang, Jaewon Lee, Seung Jae Oh, Seyoung Moon, Hong Jae Lee, Sangcheon Lee, Joo-Hiuk Son, Donghyun Kim, Kwangyeol Lee, Jin-Suck Suh, Yong-Min Huh* and Seungjoo Haam*

Materials: Calcium hydroxide, phosphoric acid, tetrachloroaurate (III) trihydrate, tetrakis (hydroxymethyl) phosphonium chloride solution, sodium hydroxide, 3-aminopropyltrimethoxysilane, potassium carbonate and formaldehyde were purchased from Sigma-Aldrich Chemicals and phosphate buffered saline (PBS, 10 mM, pH7.4) was purchased from Hyclone and used without further purification. Human immunoglobulin G (IgG) as an irrelevant antibody and FITC-labeled goat anti-human IgG were purchased from ZyMaxTM. Erbitux® was purchased from Roche Pharmacuetical Ltd. Sephacryl S-300 and calcein AM were purchased from Amersham Biosciences and Molecular Probes, respectively.

Synthesis of calcium phosphate nanoparticles (CPNs): Calcium phosphate nanoparticles (CPNs) were synthesized by a chemical precipitation and hydrothermal technique according to a previously published protocol with some modifications.[1] An aqueous solution of phosphoric acid (0.3 M, 300 mL) was added to a vigorously stirred aqueous solution of calcium hydroxide (0.25 M, 625 mL) in a dropwise manner at a rate of 1 mL/min at 60°C. After completion of the phosphoric acid addition, the pH of the suspension was adjusted to pH 7.0. After aging, CPNs were purified and collected by repeated washing with distilled water and centrifugation at 2,500 rpm for 20 minutes (repeated 5 times). The final product of CPNs was obtained by freeze-drying.

Synthesis of calcium phosphate-gold nanocomposites: Gold nanoparticles (GNPs, ~2 nm) were prepared by the reduction of tetrachlorolaurate (III) trihydrate (2 mL of 1.0 wt%) in the presence of a tetrakis (hydroxymethyl) phosphonium chloride solution (12 μL) and sodium hydroxide (0.5 mL of 1 M) solution as a reducing agent for 7 minutes at room temperature. The surface of CPNs was modified by self-assembly of 3-aminopropyltrimethoxysilane (5 μL) and CPNs (40 mg) in 5 mL of distilled water at 70^{o}C for 3 hours. The aminated CPNs were purified by centrifugation and re-dispersed in distilled water (0.5 mL). X-ray photoelectron spectroscopy (XPS) was used to confirm the synthesis of aminated CPNs. Aminated CPNs (40 mg) were stirred with an excess of GNPs (7×10^{14} particles/5 mL). The amine group at CPN surface was used as an attachment site for binding of colloidal GNPs, which then served as nucleation sites for further growth by reduction of gold salts using formaldehyde. This consequently led to the formation of a continuous and reticular gold layer. The gold salts solution was prepared by

adding potassium carbonate (25 mg) into tetrachlroloaurate (III) trihydrate (50 mL of 0.02 wt%). Two hundred μL of CPNs-GNPs solution was mixed with the gold salts solution (4 mL) and formaldehyde (80 μL) for 5 minutes. After a 2-fold reduction of gold on CPN-GNPs, CPGNs were formed and purified by repeated washing with distilled water and centrifugation at 15,000 rpm for 20 minutes (repeated 5 times).

Degradation test: The synthesized CPNs can be degraded in an acidic environment according to the following reaction (eq 1).[2] To evaluate the degradation ratio of CPNs, CPNs (4 mg) was immersed in various range of pH solution (5 mL; pH 3, 4, 5, 6 and 7) for 24 hours and transmittance was measured using UV-Vis spectroscopy at 240 nm (Figure S7). Furthermore, the amount of released calcium ions from CPGNs was investigated by inductively coupled plasma mass spectrometry (ICP-MS) at various pH conditions (pH 4, 5 and 7.4). CPGNs (5 mg/mL, 5 mL) was immersed in at each solution for 24 hours and treated with aqua regia which is 3 : 1 mixture of HCl : HNO_3, and evaporated overnight at 110°C and 4 mL of distiled water was added for measuring using ICP-MS. In Figure 1c, relative degradation ratios were calculated using the ratio of calcium ion at pH 4 or 5 to calcium ion at pH 7.4. To confirm change of plasmon peaks during CPGNs degradation, on the other hands, UV-Vis absorption spectra of CPGNs at various pH conditions (pH 3, 4, 5, 6 and 7.4) were analyzed after 120 hours.

$$Ca_{10}(PO_4)_6(OH)_2 + 2H^+ \leftrightarrow 10Ca^{2+} + 6PO_4^{3-} + 2H_2O \quad \text{(eq 1)}$$

Simulation of the extinction spectra of CPNGs: For theoretical analysis of the extinction spectra, a Mie calculation of inhomogeneous ellipsoids was conducted, assuming smooth particle geometry. The surface of the particle is described as:

$$\begin{aligned}
&\frac{x^2}{a_{(i,o)}^2+\xi}+\frac{y^2}{b_{(i,o)}^2+\xi}+\frac{z^2}{c_{(i,o)}^2+\xi}=1, \quad -c_{(i,o)}^2<\xi<\infty \\
&\frac{x^2}{a_{(i,o)}^2+\eta}+\frac{y^2}{b_{(i,o)}^2+\eta}+\frac{z^2}{c_{(i,o)}^2+\eta}=1, \quad -b_{(i,o)}^2<\eta<\infty \\
&\frac{x^2}{a_{(i,o)}^2+\zeta}+\frac{y^2}{b_{(i,o)}^2+\zeta}+\frac{z^2}{c_{(i,o)}^2+\zeta}=1, \quad -a_{(i,o)}^2<\zeta<\infty,
\end{aligned} \quad (2)$$

where a, b and c with subscripts i and o correspond to the inner and outer radii of the x, y, and z axis, respectively, and ξ, η and ζ are derived from the ellipsoidal coordinates. Note in this case that $b = c \leq a$, which corresponds to a prolate ellipsoid with a principle axis coinciding with the x axis. To obtain an extinction cross-section of the particles in response to the field in the x, y and z-axes, the polarizability, $\alpha_{(x, y, z)}$ in each axis was first calculated as:

$$\alpha_{(x,y,z)} = \frac{\upsilon((\varepsilon_2 - \varepsilon_m)[\varepsilon_2 + (\varepsilon_1 - \varepsilon_2)(L^i_{(x,y,z)} - fL^o_{(x,y,z)})] + f\varepsilon_2(\varepsilon_1 - \varepsilon_2)}{[\varepsilon_2 + (\varepsilon_1 - \varepsilon_2)(L^i_{(x,y,z)} - fL^o_{(x,y,z)})][\varepsilon_m + (\varepsilon_2 - \varepsilon_m)L^o_{(x,y,z)}] + fL^o_{(x,y,z)}\varepsilon_2(\varepsilon_1 - \varepsilon_2)}, \quad (3)$$

where the eccentricities of the inner (superscripted *i*) and outer (superscripted *o*) ellipsoids (L_x, L_y *and* L_z) are defined as:

$$L_x^{(i,o)} = \frac{a_{(i,o)}b_{(i,o)}c_{(i,o)}}{2}\int_0^\infty \frac{dq}{(a^2_{(i,o)} + q)F_{(i,o)}(q)}$$

$$L_y^{(i,o)} = \frac{a_{(i,o)}b_{(i,o)}c_{(i,o)}}{2}\int_0^\infty \frac{dq}{(b^2_{(i,o)} + q)F_{(i,o)}(q)} \quad (4)$$

$$L_z^{(i,o)} = \frac{a_{(i,o)}b_{(i,o)}c_{(i,o)}}{2}\int_0^\infty \frac{dq}{(c^2_{(i,o)} + q)F_{(i,o)}(q)}, \text{ and}$$

$$F_{(i,o)}(q) = \sqrt{(a^2_{(i,o)} + q)(b^2_{(i,o)} + q)(c^2_{(i,o)} + q)}.$$

In Eq. (3), $\upsilon = 4\pi a_o b_o c_o$ is the volume of the particle, $f = \frac{a_o b_o c_o}{a_i b_i c_i}$ is the volume fraction of the inner ellipsoid, and $\varepsilon_{(1,2,m)}$ is complex dielectric constant of: 1; inner material, 2; outer material, and m; surrounding medium, respectively. From the description of the scattered electric fields, the extinction cross-section, C_{ext} was obtained from the polarizability calculation with the following relationship:

$$C_{ext} = k\,\mathrm{Im}\{\alpha\}, \quad (5)$$

where the wave vector k is defined as $k = 2\pi/\lambda$.

The extinction spectra of three different types of plasmonic core-shell nanoparticles (ellipsoidal CPGNs, spherical CPGNs and spherical silica-gold core-shell structures) were calculated for comparison. The dielectric constants of gold and water were obtained from the experimental measurements and were interpolated in the wavelengths of interest (400 ~ 1,200 nm).[3] The refractive index of CPNs (1.651) and silica nanoparticles (1.460) were assumed to be constant over the range of wavelengths. The major axis (a) and minor axis (b = c) of the ellipsoidal CPNs was 60 nm and 10 nm, respectively. The thickness of gold shell for CPGNs was 10nm for consistence with the experimental data. The both extinction spectra of the spherical CPGNs and silica gold nanoshells (a = b = c = 18.2 nm) were calculated based on the same core volume and gold shell thickness with the ellipsoidal CPGNs. In Figure S6, the ellipsoidal CPGNs exhibited higher extinction spectra at NIR region rather than spherical CPGNs and silica gold nanoshells.

Conjugation of ERB with CPGNs: In order to conjugate ERB (Erbitux®, anti-EGFR antibody) with CPGNs, 2 mg of ERB was mixed with 4 mg of CPGNs in the PBS (pH 7.4, 10 mM) at 4°C.

After 4 hours, ERB-CPGNs were purified with a Sephacryl S-300 column. The quantity of conjugated ERB onto the surface of CPGNs was evaluated by a BCA protein assay (Thermo Fisher Scientific Inc.) and 20 equivalent ERB was conjugated on to CPGNs. Similarly, for control experiments, the irrelevant (IRR) human immunoglobulin G (IgG) antibody was conjugated with CPGNS. The IRR-conjugated CPGNs was synthesized with the same manner as described for ERB-CPGNs.

Cellular affinity test: The epidermoid carcinoma A431 and MCF7 cell lines were obtained from American Tissue Type Culture (ATCC, Rockville, MD) and cultured. Briefly, the cells (1×10^5 cells/mL) were seeded in 100 ϕ Corning culture dishes (10 mL/dish) with Dulbecco's Modified Eagle Medium supplemented with 10% fetal bovine serum (FBS) and 1% antibiotics and incubated at 37 ^oC in a humidified atmosphere composed of 5% CO_2. Fluorescence-activated cell sorting (FACS) analysis was performed to determine the affinity of ERB-CPGNs (1 mg/mL, 200 μL) for A431 and MCF7 cells, respectively. A431 and MCF7 cells were washed with buffer (2 % FBS and 0.02 % NaN_3 in PBS) and then the cells were incubated with ERB-CPGNs and IRR-CPGNs for 1 hour at 4 ^oC, respectively. The temperature was maintained at 4^oC in order to avoid non-specific binding through endocytosis without receptor-mediated uptake. The treated cells were washed three times with an FITC-labeled goat anti-human IgG for 45 minutes at 4^oC in the dark room. Finally, the cells were suspended in 400 μL PBS and stored at 4^oC prior to FACS analysis (Becton Dickinson, Mountain View, California, USA).

Investigation of therapeutic efficacy: A431 and MCF7 cells (4×10^3 cells/well) were incubated in 96-well plates for 24 hours. Target cells were incubated with ERB-MGNCs or IRR-MGNCs (1 mg/mL, 100 μL) at 37^oC. After 4 hours, an equal volume of 10% FBS was added to each of the wells, and the cells were incubated for an additional 72 hours. During exposure to an NIR laser, thermographic data were recorded with an infrared thermal camera (Thermographic System, AXT100) with time intervals of 1 second over a course of 5 minutes, and the temperature of the cells was then calculated from the images using Thermographic System software. After exposure to an NIR laser (820 nm and 25 W/cm^2 for 5 minutes), the cells were incubated for 2 hours at 37^oC. The distribution of live and dead cells after staining with a calcein AM (l μM) was observed using a fluorescence microscope. The therapeutic efficacies were determined by calculating the differences between cell viabilities under treated and non-treated conditions (n=3).

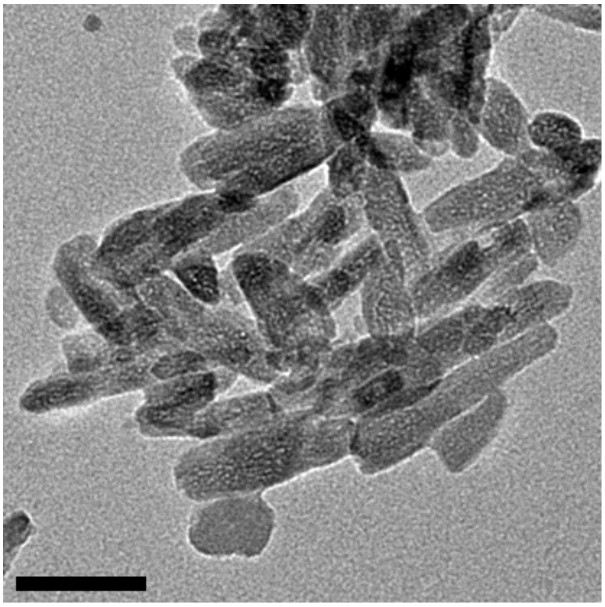

Figure S1. TEM images of CPNs (scale bar means 100 nm).

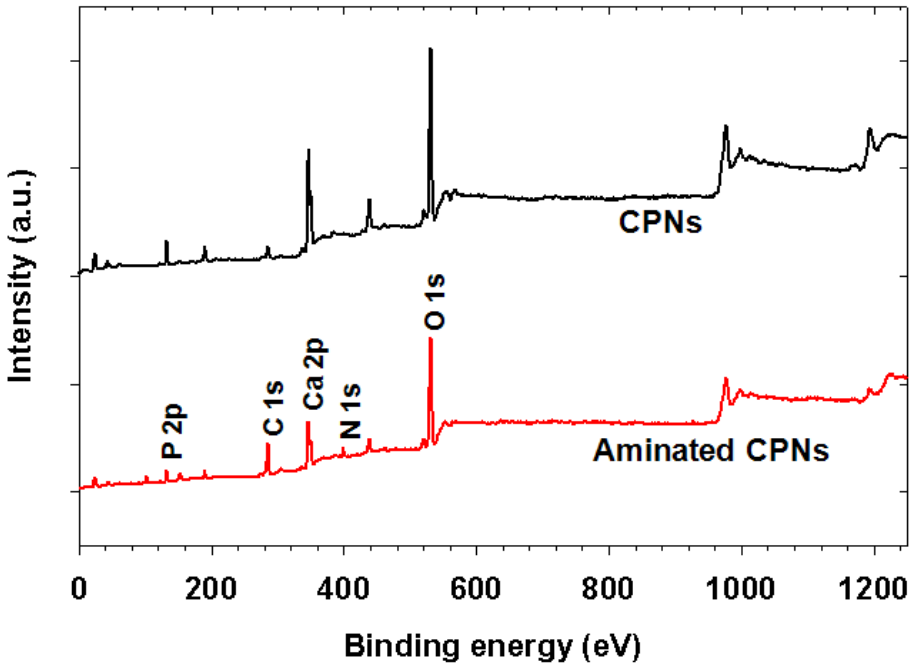

Figure S2. X-ray photoelectron spectroscopy for CPNs and aminated CPNs (CPNs-NH_2).

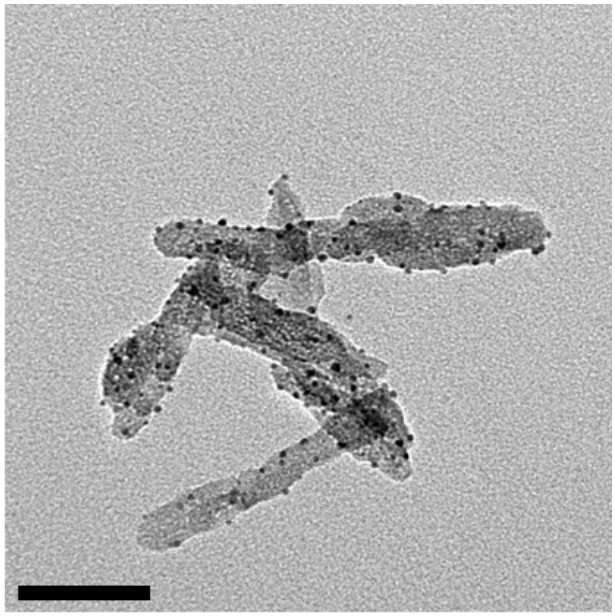

Figure S3. TEM images of CPNs-GNP (scale bar means 100 nm).

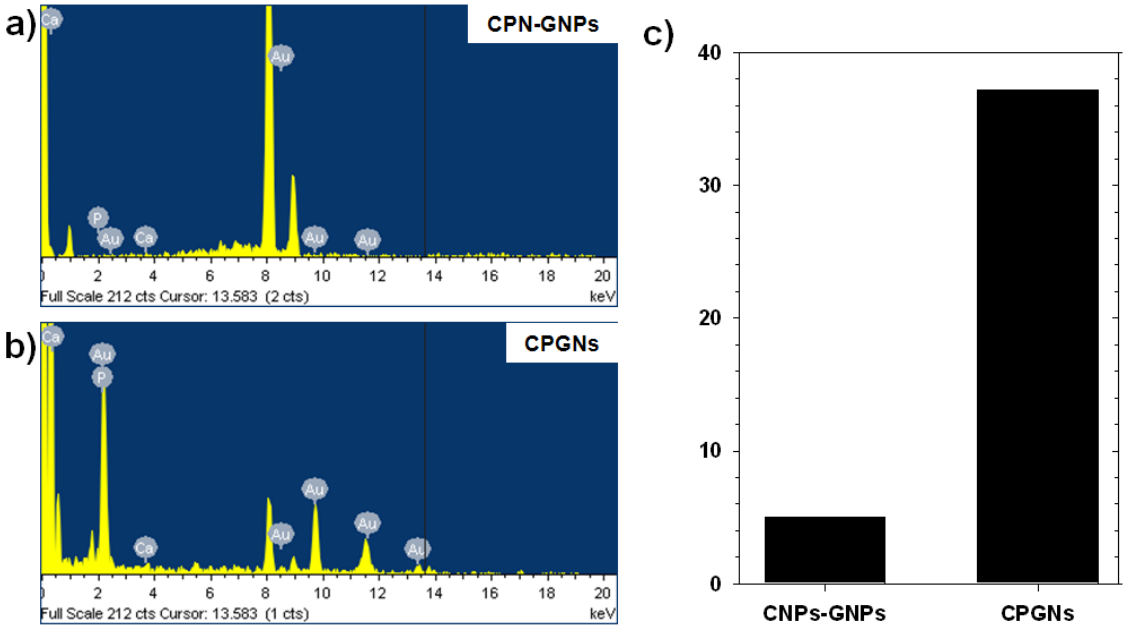

Figure S4. Energy-dispersive X-ray spectroscopy spectra of a) CPNs-GNP and b) CPGNs, and c) Au compositions of CNPs-GNPs and CPGNs, repectively.

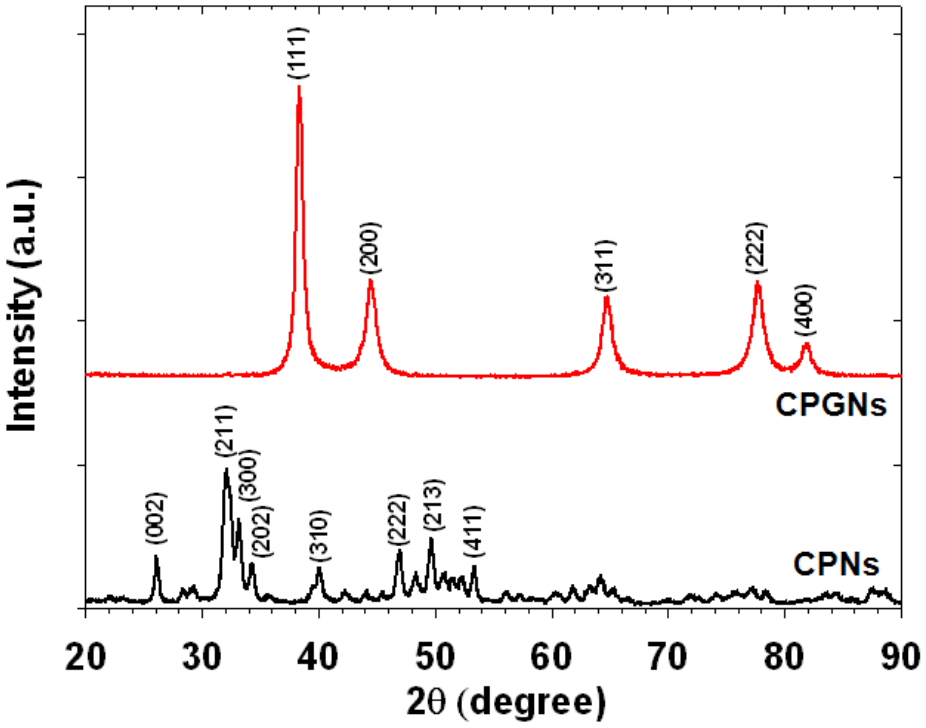

Figure S5. X-ray diffraction patterns of CPGNs and CPNs.

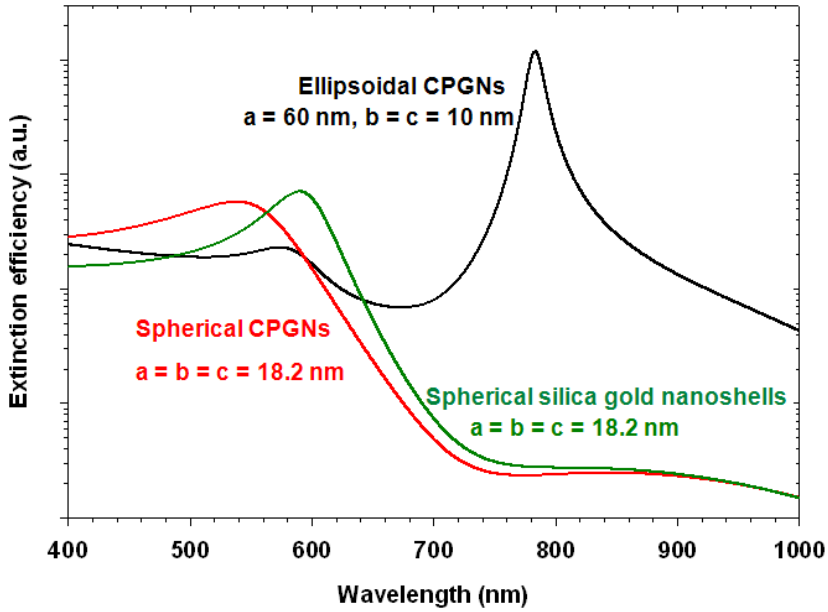

Figure S6. Comparison of the calculated extinction spectra for ellipsoidal CPGN, spherical CPGN and spherical silica-gold core-shell (gold thickness = 10 nm).

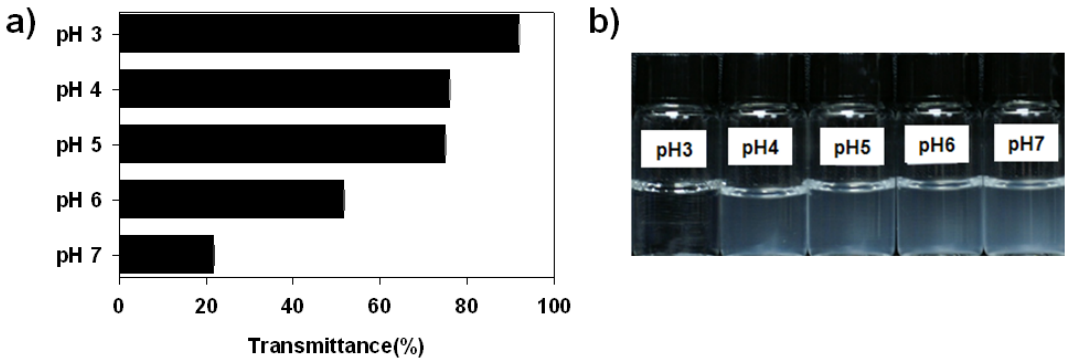

Figure S7. a) Transmittance of CPNs at various pH conditions to examine the potential for biodegradability. b) The photograph show the turbidities of CPN solutions according to the degree of degradation (pH 3 ~ 7).

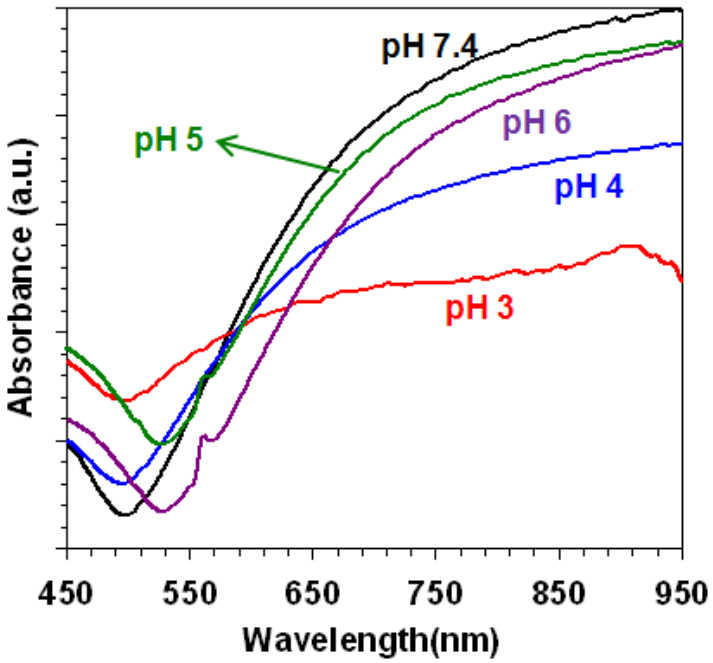

Figure S8. UV-Vis absorbance spectra of CPGNs at pH 3, 4, 5, 6 and 7.4 after 120 hours.

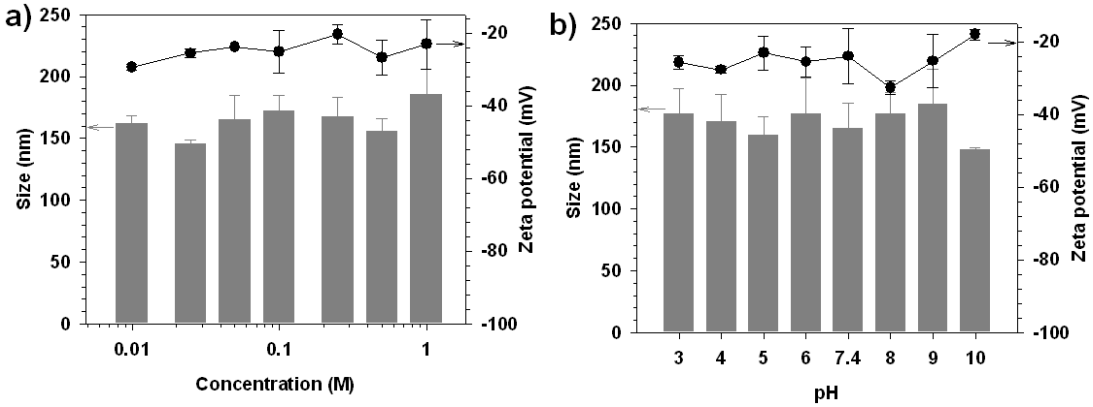

Figure S9. Particle size and zeta potential of ERB-CPGNs plotted against various (a) pH conditions and (b) NaCl concentrations.

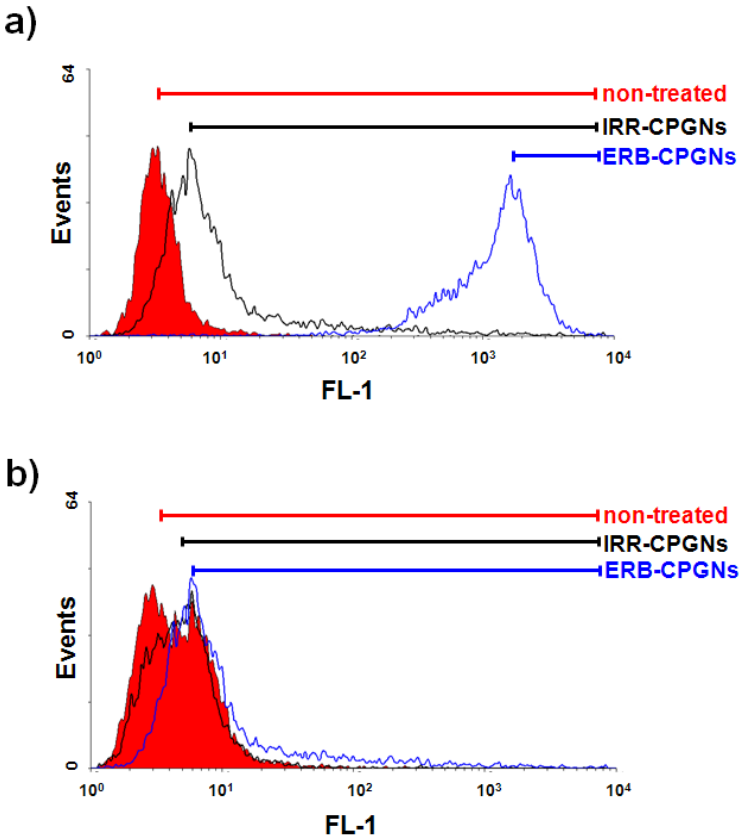

Figure S10. FACS analysis of a) A431 and b) MCF7 cells incubated with ERB-CPGNs and IRR-CPGNs, respectively.

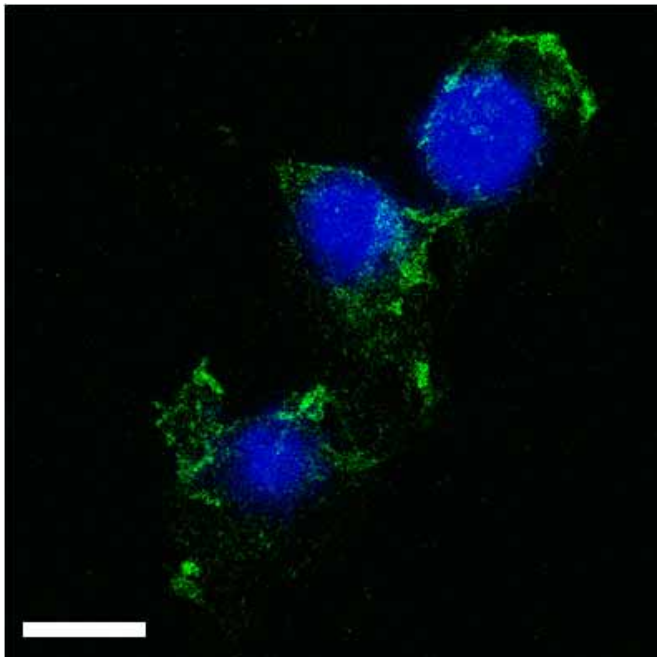

Figure S11. Confocal microscope image of A431 cells treated with ERB-CPGNs (scale bar means 5 μm).

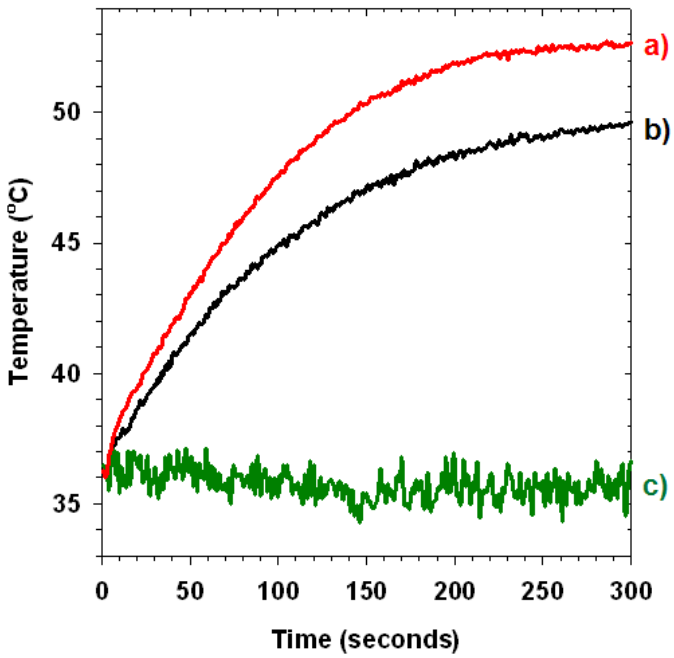

Figure S12. Temperature variations for incubation wells of a) only CPGNs solution, b) A431 cells treated with ERB-CPGNs and c) non-treated A431 cells after NIR laser irradiation (820 nm and 25 W/cm^2 for 5 minutes), respectively.

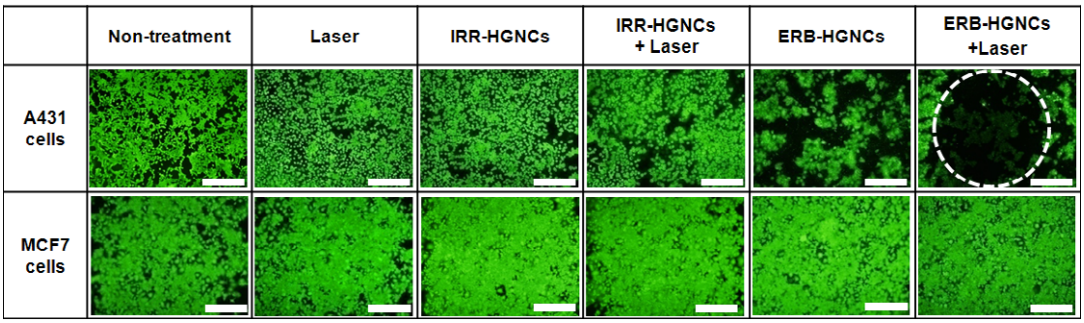

Figure S13. Fluorescence microscopic images of A431 or MCF7 cells stained with calcein AM for each after treatment; non-treatment, laser only, IRR-CPGNs, IRR-CPGNs + laser, ERB-CPGNs and ERB-CPGNs + laser, respectively (scale bar means 1 mm).

References

1. H. J. Lee, H. W. Choi, K. J. Kim and S. C. Lee, *Chem. Mater.*, 2006, **18**, 5111-5118.
2. X. Wang, A. Klocke, B. Mihailova, L. Tosheva and U. Bismayer, *J. Phys. Chem. B*, 2008, **112**, 8840-8848.
3. E. D. Palik, *Handbook of Optical Constants of Solids* Academic Press, 1991.